INTERNATIONAL JOURNAL FOR NUMERICAL METHODS IN FLUIDS, VOL. 25, 1083–1103 (1997)

EVOLUTION OF FLOW STRUCTURE IN IMPINGING THREE-DIMENSIONAL AXIAL AND RADIAL JETS

H. LASCHEFSKI, T. CZIESLA AND N. K. MITRA*

Institute für Thermo- und Fluiddynamik, Ruhr-Universität Bochum, D-44780 Bochum, Germany

SUMMARY

Direct numerical simulations of the flow field of an element of banks of impinging axial and radial slot jets for different Reynolds number are presented. Simulations have been obtained from the solution of the Navier–Stokes equations. Results show for the chosen geometry a transition from steady to periodic to chaotic flow with increasing Reynolds number. The transition Reynolds number is nearly 50% smaller for the radial jet than for the axial jet. Period doubling has been observed for both cases, but only the radial jet shows periodic windows of chaos. © 1997 John Wiley & Sons, Ltd.

Int. J. Numer. Meth. Fluids, **25**: 1083–1103 (1997)

No. of Figures: 19 No. of Tables: 2 No. of References: 10.

KEY WORDS: radial jets; axial jets; direct numerical simulation

INTRODUCTION

Rows of impinging jets issuing out of rectangular slots or round tubes are often used in industry for heating, cooling or drying of product surfaces. Often these jets are turbulent, but, in some applications (e.g. electronic cooling) they can be laminar. Laminar jets discharging out of a round or a rectangular feed tube eventually become turbulent[1] when the Reynolds number is larger than 30. The distance at which the transition takes place depends on *Re*. Laminar jets impinging on a plate can undergo transition depending on the Reynolds number and the distance between the jet and the plate before impingement. Relaminarization may occur close to the impingement point and a second transition may occur as the flow develops as a wall jet after impingement. This can be seen from the two peaks of the measured local mass transfer rate on the impingement plate.[2]

Numerical computations of flow fields of laminar[3] and turbulent[4] jets have been reported. However, the flow field of an impinging jet may contain laminar, transitional and turbulent zones. A direct numerical simulation for such a flow will be a meaningful tool to study the structure.

In a previous paper we investigated the evolution of the flow structure of impinging axial and radial jets issuing out of a round feed tube.[5] The radial jet issues from the side of the round tube and

*Correspondence to: N. K. Mitra, Institute für Thermo- und Fluiddynamik, Ruhr-Universität Bochum, D-44780 Bochum, Germany.

Contract grant sponsor: Deutsche Forschungsgemeinschaft

CCC 0271–2091/97/091083–21 $17.50

Received July 1996
Revised December 1996

reattaches on the impingement plate in the form of an umbrella. The computational results of Laschefski *et al*[5] showed that both types of jets could be steady at low Reynolds number. As *Re* was increased, the jets became oscillatory. The frequency and amplitude of oscillations changed with increasing *Re*. The oscillation started with one dominant frequency and a moderate amplitude. As *Re* was increased further, more frequencies appeared and the amplitudes at some of the frequencies became larger. As *Re* was increased still further, aperiodic flow resulted. A fast Fourier analysis of the time series of a velocity component at a chosen point failed to show any dominant frequency for the aperiodic flow. At even higher *Re* the numerical solution failed to converge. This change from steady to aperiodic solution described the transition from laminar to turbulent flow. Computational experiments showed that the failure to converge could be postponed to higher Reynolds numbers by the use of finer grids. Although both types of jets gave qualitatively the same flow, the radial jet appeared to be less stable since it produced the transition to periodic and aperiodic flows at lower Reynolds numbers than the axial jet.

In the previous computations[5] the flow was modelled as axisymmetric in order to reduce computational effort. This naturally puts a constraint on the actual physics of transition. The purpose of the present work is a similar study of the flow structure evolution but of three-dimensional impinging jets. We will consider a bank of slot jets issuing out of rectangular feed tubes or nozzles either axially or 'radially', i.e. from the sides of the feed tubes. Only an element consisting of one jet of the bank will be handled in the computational domain. Some preliminary results have already been presented.[6] Here we present in detail the evolution of the flow structure.

The transition to chaos as a function of the Reynolds number in an unforced flow has been numerically investigated by Pulliam and Vastano,[7] who computed the compressible flow around a two-dimensional aerofoil at a Mach number of 0·2 and an angle of attack of 20°. They found that the system undergoes a period-doubling bifurcation as the Reynolds number is increased from 800 to 1600 with periodic windows. The present work follows closely the work of Pulliam and Vastano.[7] However, the flow here is three-dimensional. To the authors' knowledge, no experimental or computational study of the transition to chaos of an impinging jet flow has ever been reported. Hence a comparison of the present results with other works could not be performed.

BASIC EQUATIONS AND METHOD OF SOLUTION

Computational Domain

Figures 1(a) and 1(b) show three-dimensional schematic diagrams of the banks of axially and radially impinging slot jets. The corresponding front views are also shown. In Figure 1(a), jets issue from rectangular parallel slots of width B. The distance (pitch) between the axes of two neighbouring parallel slots is L_T the length of each slot is $2l$ and the height of the slot exit above the impinging plate is h. The jets are semi-enclosed and the height of the enclosing plate above the impingement plate is H. For the axially discharging jet (Figure 1(a)) the fluid after hitting the impingement plate moves sideways only a small distance, as it is restrained by the neighbouring jets. The fluid moves out in directions normal to the paper (y-axis in Figure 1(a)). In contrast with the axial jet (Figure 1(a)), for the 'radial' or knife jet of Figure 1(b) the jet fluid discharges from the sides. The height h in this case is the distance between the impingement plate and the midpoint of the sideways slot. The height of the slot is $B/2$, so the total flow cross-section of the two radial slots is equal to the flow cross-section of the axial jet. The computational domains consisting of an element are depicted by broken lines in Figures 1(a) and 1(b)).

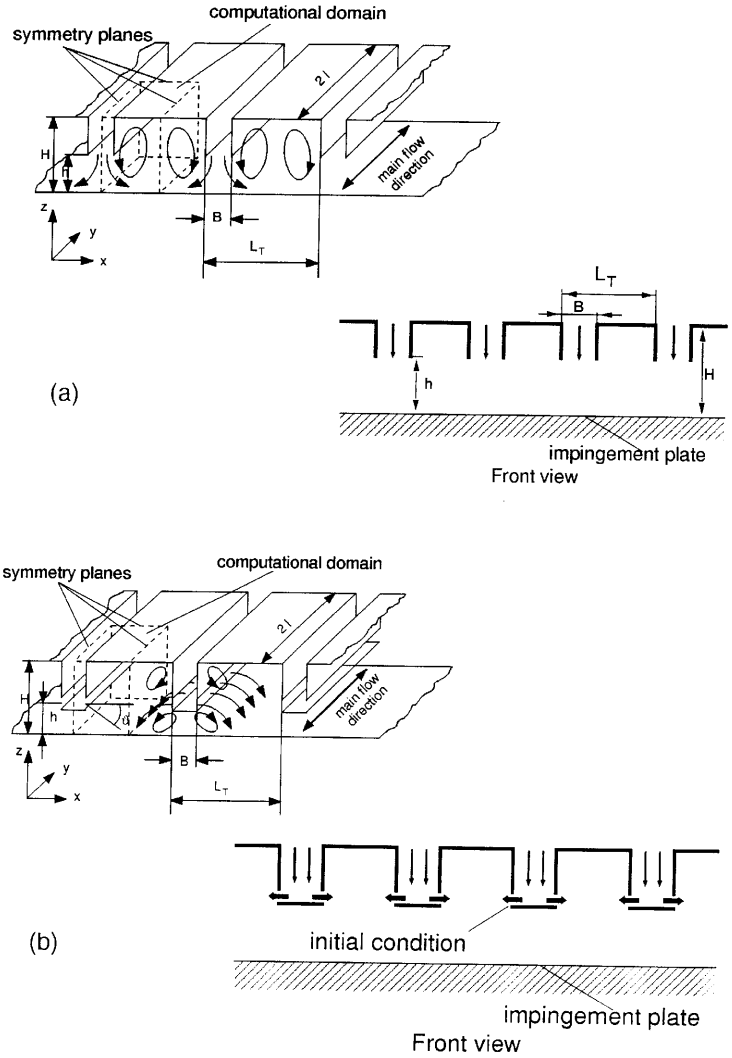

Figure 1. Schematic diagrams of rectangular (a) axial and (b) radial jets together with front views. The three-dimensional computational domains are shown by broken lines

Basic Equations

The jet fluid is assumed to be incompressible with constant properties and the jets are discharging in an ambience of the same fluid. The flow field is described by the Navier–Stokes equations, which in non-dimensional Cartesian index form for non-steady three-dimensional flow read as

$$\frac{\partial V_i}{\partial x_i} = 0, \tag{1}$$

$$\frac{\partial V_j}{\partial t} + \frac{\partial (V_i V_j)}{\partial x_i} = -\frac{\partial p}{\partial x_i} + \frac{1}{Re}\nabla^2 V_j. \tag{2}$$

Here lengths have been non-dimensionalized with $2B$ and velocity components with V_∞, the average exit velocity of the slots. The pressure is non-dimensionalized by dividing by ϱV^2_∞, where ϱ is the density. The Reynolds number is defined as $Re = V_\infty\ 2B/v$, where v is the kinematic viscosity.

Boundary Conditions

No-slip boundary conditions on solid walls have been used. Symmetry conditions have been used on symmetry planes; see Figures 1(a) and 1(b).

At the inlet, i.e. at the exit from the slot, either a uniform or a fully developed form of velocity profile can be assumed. We have assumed uniform flow (top-hat profile). The boundary condition at the exit plane is a problem, because the ambient fluid will be entrained in the computational domain across the upper part of the exit plane, whereas across the lower part the jet will discharge in the ambient. At this plane the first derivatives of velocity components are set equal to zero and the pressure is taken to be constant.[5]

Computational Scheme

The basic equations have been solved by a pressure-based finite volume code FIVO developed by the present authors. This code uses SIMPLE C[9] pressure correction. Collocated grids with momentum interpolation are used.[8]

Computations have been performed with 71,400 ($34 \times 42 \times 50$) and 53,376 ($66 \times 82 \times 98$) equidistant grid points, corresponding to grid sizes of 0·0625 and 0·03125 respectively. A detailed study of the grid size dependence of the present results has not been performed with still finer grids, because it would require a prohibitively large computer capacity. Pulliam and Vastano[7] did do a detailed study of grid dependence, but they employed a two-dimensional geometry. We performed a grid dependence study with the present code for a non-steady flow in a two-dimensional channel with a square cylinder in it. Results with a grid of $\Delta x = 0{\cdot}05$, $\Delta y = 0{\cdot}04$ (202×102) show that the Strouhal number of the vortex street differs from the grid-independent Strouhal number by less 4%.[5] Although the code can calculate time-implicit difference formulae, time-explicit discretization has been used in the present work. The time step has been calculated from the CFL condition.[5] A reduction of the time step by 50% from the allowable step size shows less than 3% difference in Strouhal number for the square cylinder in the channel case. The details of the computational scheme, the difference formula using the deferred correction technique for the convective fluxes and the implementation of the constant pressure boundary condition can be found in Reference 5. The code has been validated by calculating a plane jet flow and comparing the numerical results with analytical results.[5]

RESULTS AND DISCUSSION

The flow structure depends on the geometrical parameters (H, B, h, l and L_T) and the Reynolds number Re. In this work we study the effect of Re and keep the geometrical parameters fixed at $h/B = 2$, $H/B = 6$, $l/B = 5$ and $L_T/B = 8$. These values are typical for industrial jets.[2]

The computations were started at low Re (normally 150). The computed flow field was steady. The fluid coming out of the slot hits the plate and then turns around an axis normal to the plane of the paper in Figure 1(a) (y-axis), as it cannot move in the lateral direction (x-direction) owing to the neighbouring jets. Thus the mainstream forms a longitudinal vortex as it comes out of the computational domain in the y-direction; see Reference 10 for figures of the velocity field and surface streamlines.

Then Re was increased stepwise with a step size of five. It was found that the axial jet remained steady at $Re = 335$, but at $\mathrm{Re} = 338$ the flow bifurcates to a time-periodic solution. For this case the

axis of the longitudinal vortex oscillates sideways periodically. The bifurcation Re of 338 was obtained by noting that $Re = 340$ gave a periodic solution. Re was increased by a step size of one from 335 and the previous solution was used as the starting solution. Since we solved non-steady equations, the computational results signify that for $Re < 338$ the flow becomes time-asymptotically steady, whereas for $Re = 338$ it evolves to a limit cycle or periodic attractor. This was recognized by Fourier-analysing the time series of the u-velocity component at a point in the middle of the flow field. Figure 2 shows for $Re = 338$ the time series of u, the time delay reconstruction[7] and the Fourier-analysed power density against the Strouhal number $S = f\,2B/V_\infty$, where f is the frequency.

We notice that the dominant S is approximately 0·0078 and the other two weak frequencies are represented by $S = 0{\cdot}015$ and 0·022. It is possible that at some smaller Re a periodic flow with one dominant frequency resulted. This could not be verified unless a much finer grid could be used. If Re is now raised further, the frequencies become larger, although the bandwidths of individual frequencies become narrower. Figures 3–5 show the time series, delay reconstruction and frequency spectrum at $Re = 360$, 400 and 412 respectively. The dominant Strouhal number has changed from

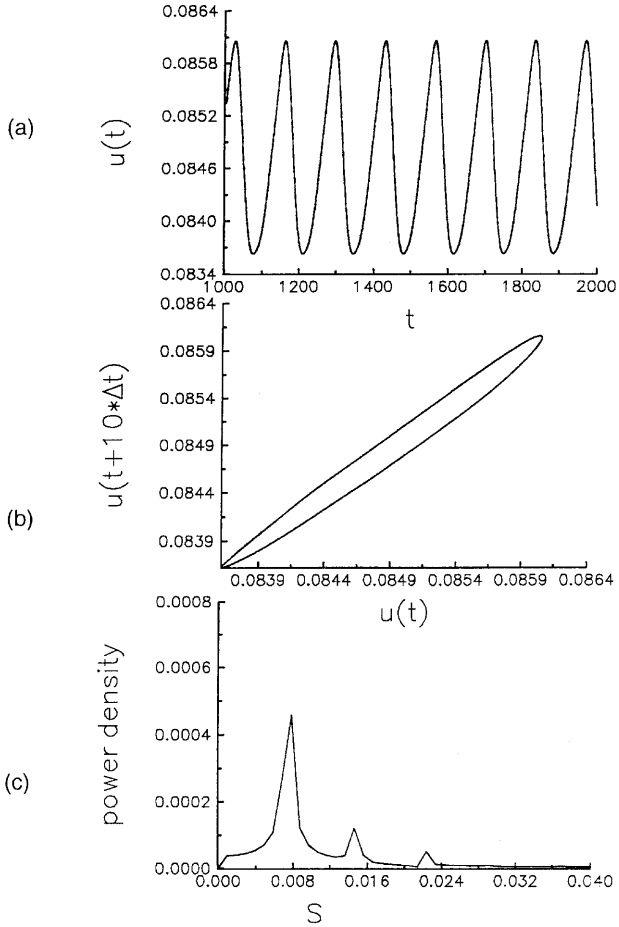

Figure 2. Velocity component $u(t)$ of axial jet for $Re = 338$: (a) time series; (b) time phase diagram; (c) Fourier analysis showing power density against Strouhal number S

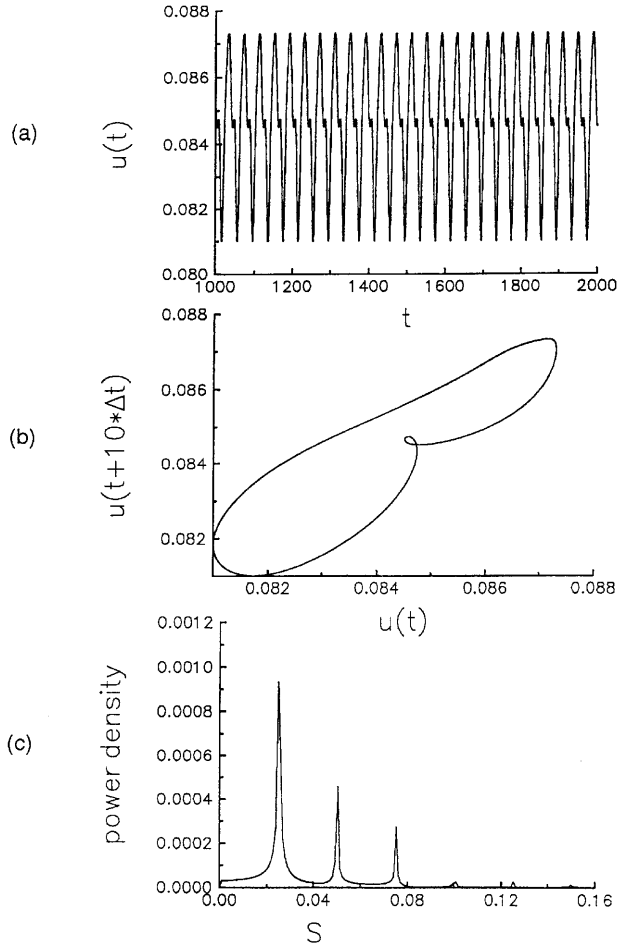

Figure 3. Velocity component $u(t)$ of axial jet for $Re = 360$: (a) time series; (b) time phase diagram; (c) fourier analysis showing power density against Strouhal number S

0·02 to 0·04. At $Re = 360$ the dominant Strouhal numbers are 0·025, 0·05 and 0·075. At $Re = 412$ there is only one dominant frequency with a Strouhal number of 0·045.

At $Re = 414$ a dramatic change in the flow field appears; see Figure 6. First we notice a period doubling, with Strouhal number 0·024. The flow structure tends to be chaotic. This tendency continues at $Re = 420$ (Figure 7) and $Re = 435$ (Figure 8). For the latter Re the flow has become turbulent.

Figure 9 shows the dominant Strouhal number against Re. Table I presents the values of S. In the chaotic regime ($Re \geqslant 414$) the dominant frequency is the one with the largest power density. The dominant S increases with Re steadily until a sudden period doubling appears. This manifests itself as a discontinuous jump condition and signifies chaos.

For the radial jets we carried out similar investigations. Steady flow was obtained at $\mathrm{Re} = 208$. At $\mathrm{Re} = 210$ the flow was periodic with a dominant Strouhal number of 0·047; see Figure 10. At $Re = 212$ the picture remains similar, except that the Strouhal number has become 0·058; see Figure 11. As Re increase further to 215, period doubling is observed; see Figure 12. The dominant

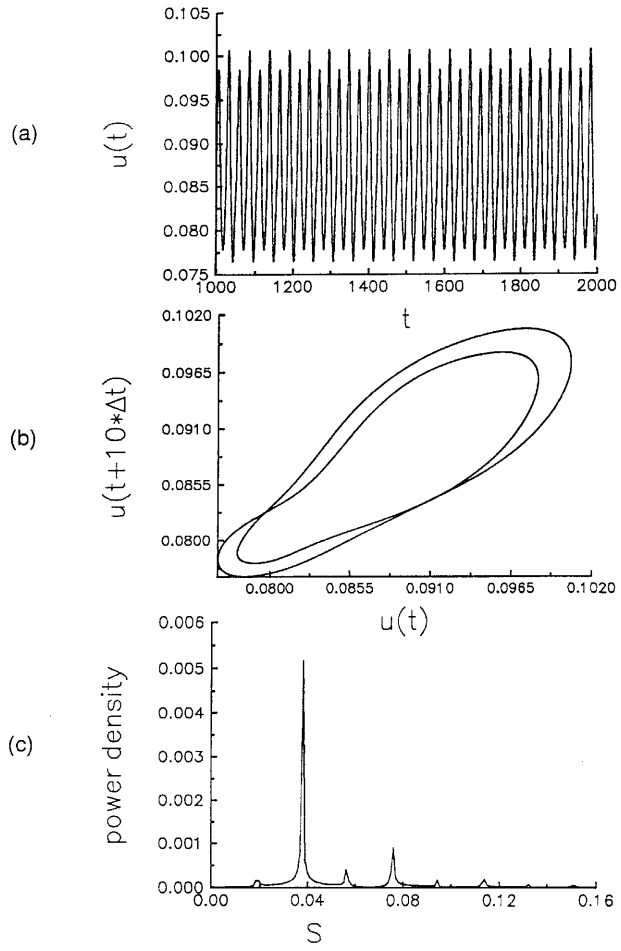

Figure 4. Velocity component $u(t)$ of axial jet for $Re = 400$: (a) time series; (b) time phase diagram; (c) Fourier analysis showing power density against Strouhal number S

frequency is 0·029 and Figure 12 shows a chaotic flow. The time-delay phase diagram did not close properly. With a further increase in Re to 220 the flow again became periodic (Figure 13) with a dominant S of 0·028. At $Re = 230$ (Figure 14), although a dominant frequency still exists, the flow has become closer to chaotic; see the phase diagram in Figure 14. At $Re = 240$ the flow has again become periodic; Figure 15. At $Re = 245$ the onset of chaos can again be noticed; see Figure 16. At larger Re (e.g. 248, 250) the flow remains chaotic with one dominant frequency; see Figure 17 for $\mathrm{Re} = 250$. At $Re = 275$ the dominant frequency disappears and the flow should treated as fully turbulent; see Figure 18. see Figure 19 again shows the dominant Strouhal number against the Reynolds number. Table II presents the exact values of S. We notice the first period-doubling discontinuity at $Re = 212$. The flow evolves to a final chaotic state through two intermediate periodic windows. For the axial jet such periodic windows of chaos have not been observed.

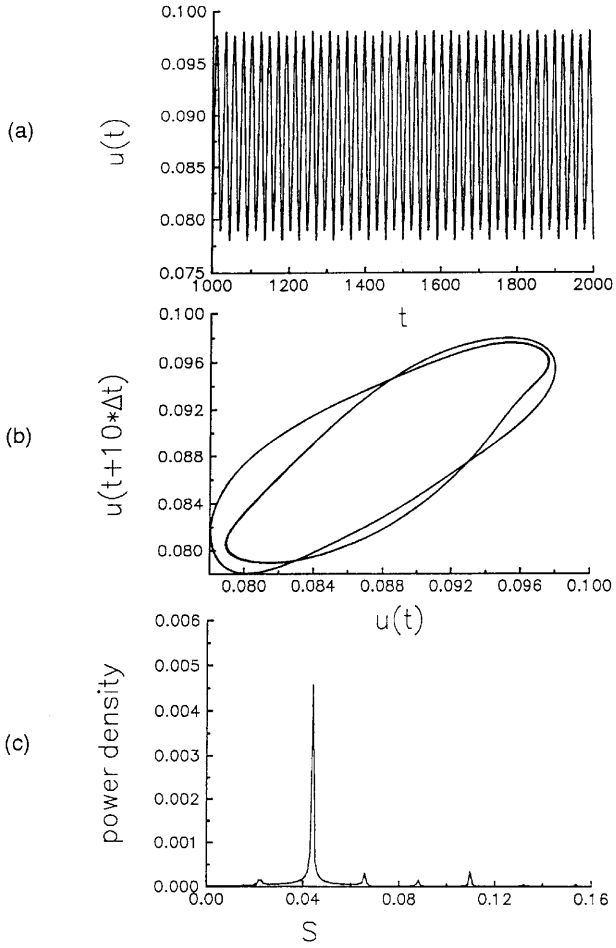

Figure 5. Velocity component $u(t)$ of axial jet for $Re = 412$: (a) time series; (b) time phase diagram; (c) Fourier analysis showing power density against Strouhal number S

CONCLUDING REMARKS

Numerical computations of three-dimensional non-steady flow fields of impinging axial and radial jets showing a sequence of flow states leading from steady to periodic to chaotic flow via a period-doubling mechanism with increasing Reynolds number are reported for the first time. For radial jet simulations, periodic windows leading to chaos have been observed. The present study follows in the footsteps of Pulliam and Vastano[7] and shows qualitatively similar results. However, because of the three-dimensional computation in the present case, the influence of mesh refinement has not been as

Table I. Dominant Strouhal number against Reynolds number for axial jet

Re	338	360	380	390	400	405	408	410	412	414	416	420	425
S	0·008	0·025	0·031	0·034	0·038	0·041	0·042	0·044	0·045	0·048	0·024	0·024	0·024

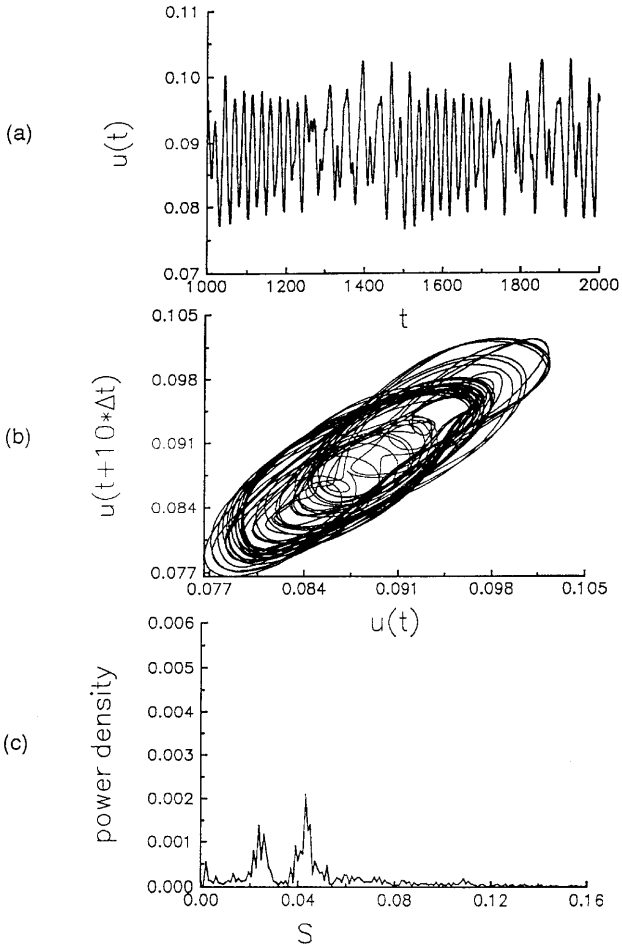

Figure 6. Velocity component $u(t)$ of axial jet for $Re = 414$: (a) time series; (b) time phase diagram; (c) Fourier analysis showing power density against Strouhal number S

Table II. Dominant Strouhal number against Reynolds number for radial jet

Re	*S*	
210	0·047	periodic
212	0·058	periodic period
215	0·029	chaotic doubling
220	0·028	periodic
230	0·031	chaotic
240	0.028	periodic
245	0·029	chaotic
250	0·035	chaotic
270	0·039	chaotic
275	—	turbulent

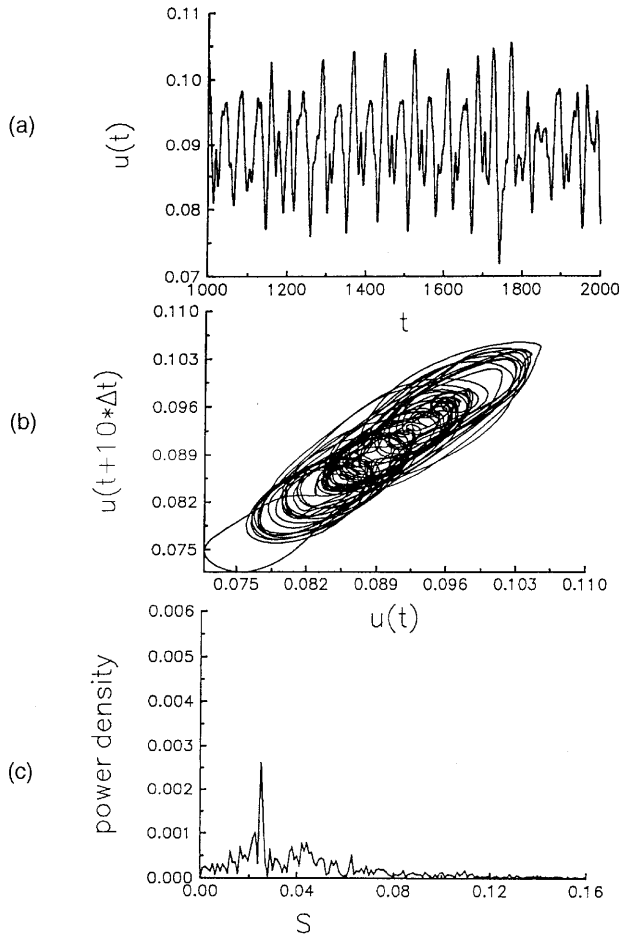

Figure 7. Velocity component $u(t)$ of axial jet for $Re = 420$: (a) time series; (b) time phase diagram; (c) Fourier analysis showing power density against Strouhal number S

rigorously studied as in Reference 7. It must also be pointed out that the computed Re for transition to chaos (or turbulence) is dependent on numerical errors. However, the results show the correct trend. Hence they may encourage further research along this new avenue of non-linear stability theory.

ACKNOWLEDGEMENT

This work has been supported by the Deutsche Forschungsgemeinschaft.

APPENDIX: LIST OF SYMBOLS

B slot width
f frequency
h height of slot exit above impingement surface
H height of enclosing plate above impingement surface
l half-length of slot

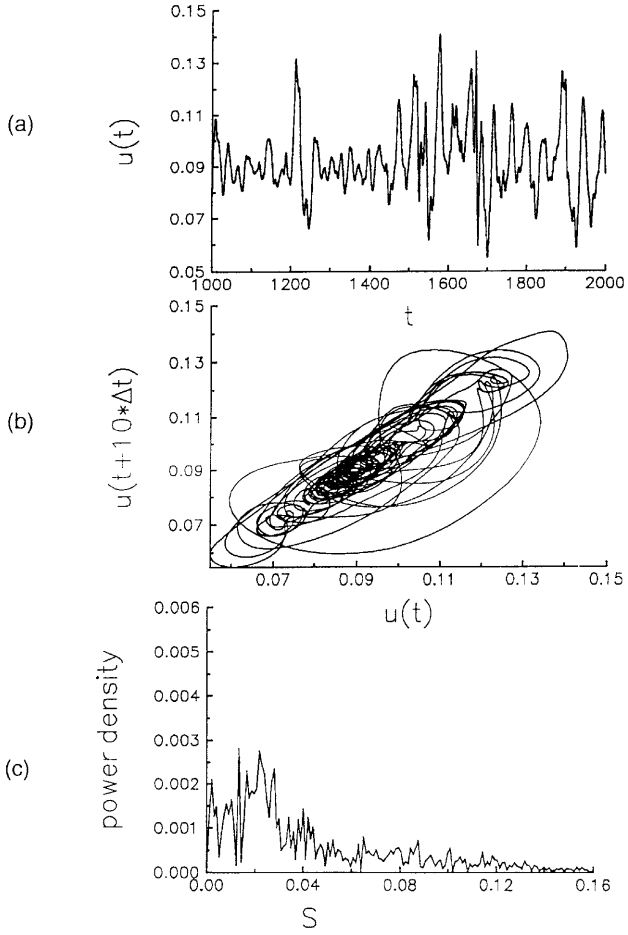

Figure 8. Velocity component $u(t)$ of axial jet for $Re = 435$: (a) time series; (b) time phase diagram; (c) Fourier analysis showing power density against Strouhal number S

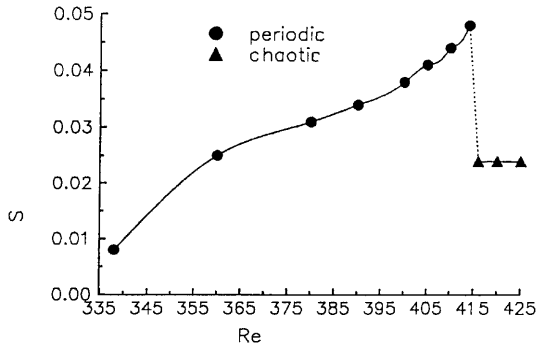

Figure 9. Dependence of dominant Strouhal number of axial jet on the Reynolds number

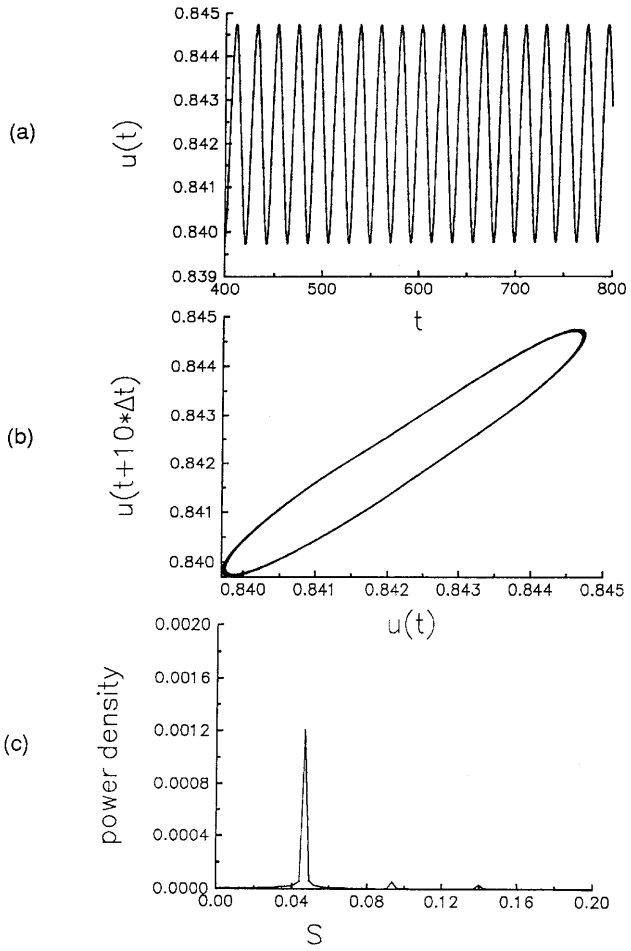

Figure 10. Velocity component $u(t)$ of radial jet for $Re = 210$: (a) time series; (b) time phase diagram; (c) Fourier analysis showing power density against Strouhal number S

L_T slot pitch
p pressure
Re Reynolds number ($= V_\infty\ 2B/v$)
S Strouhal number ($= f\,2B/V_\infty$)
t time
V_j jth velocity component
V_∞ average velocity at slot exit
x_i ith cartesian co-ordinate

Greek letters

v kinematic viscosity
ρ density

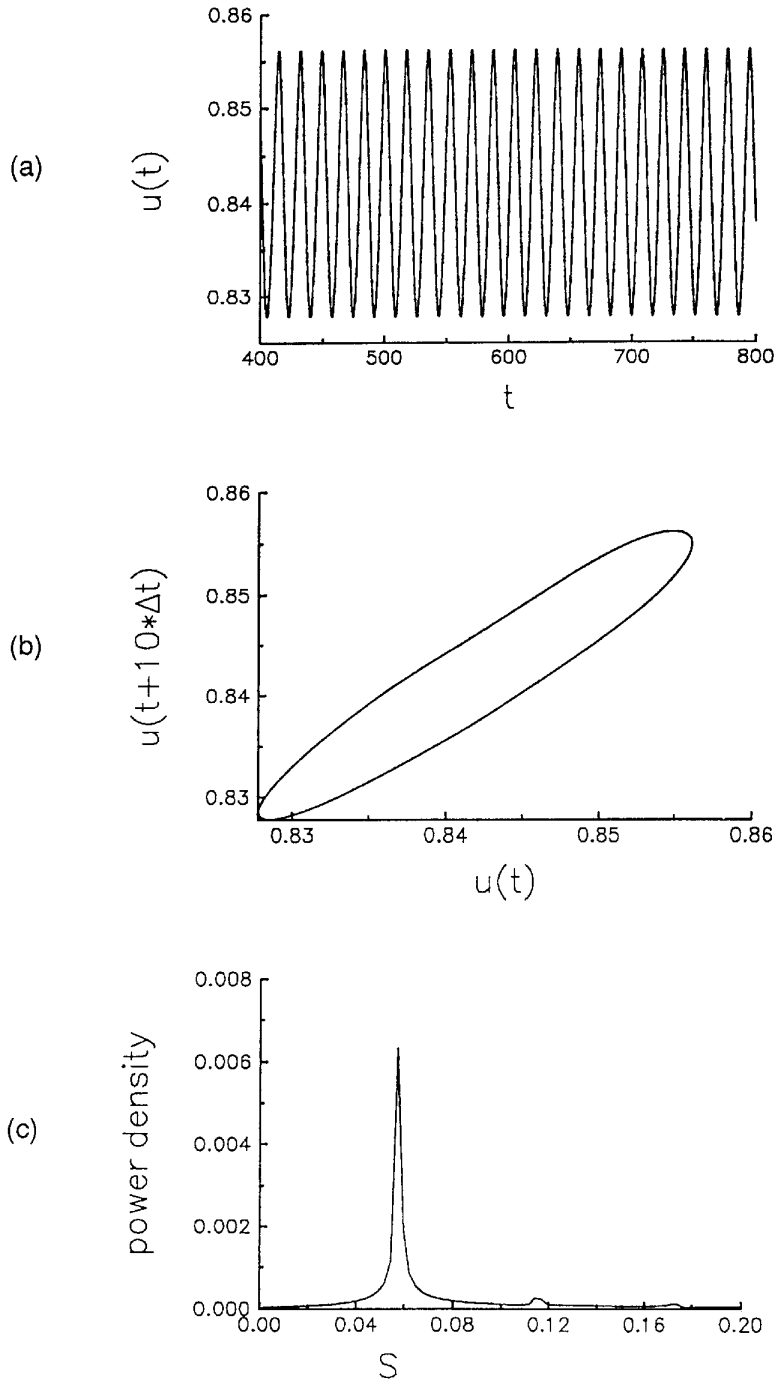

Figure 11. Velocity component $u(t)$ of radial jet for $Re = 212$: (a) time series; (b) time phase diagram; (c) Fourier analysis showing power density against Strouhal number S

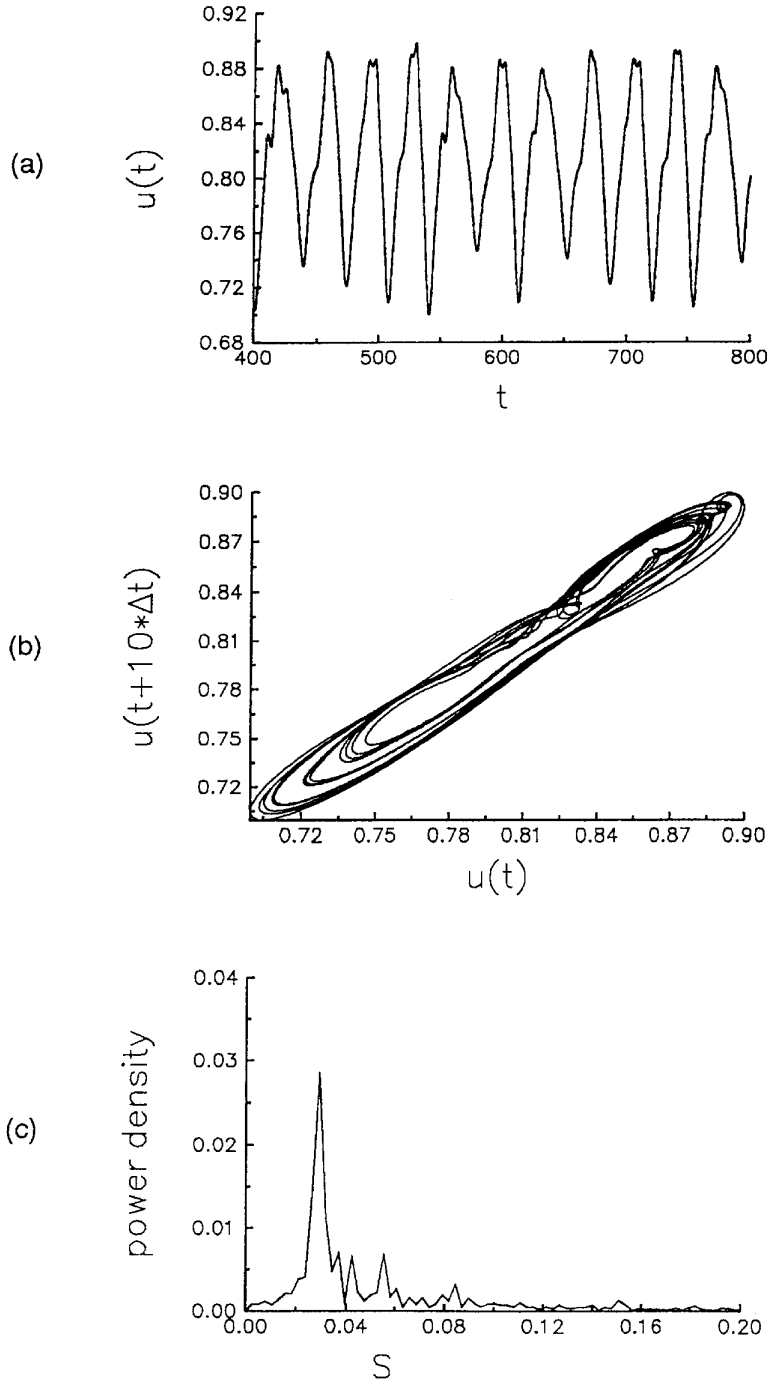

Figure 12. Velocity component $u(t)$ of radial jet for $Re = 215$: (a) time series; (b) time phase diagram; (c) Fourier analysis showing power density against Strouhal number S

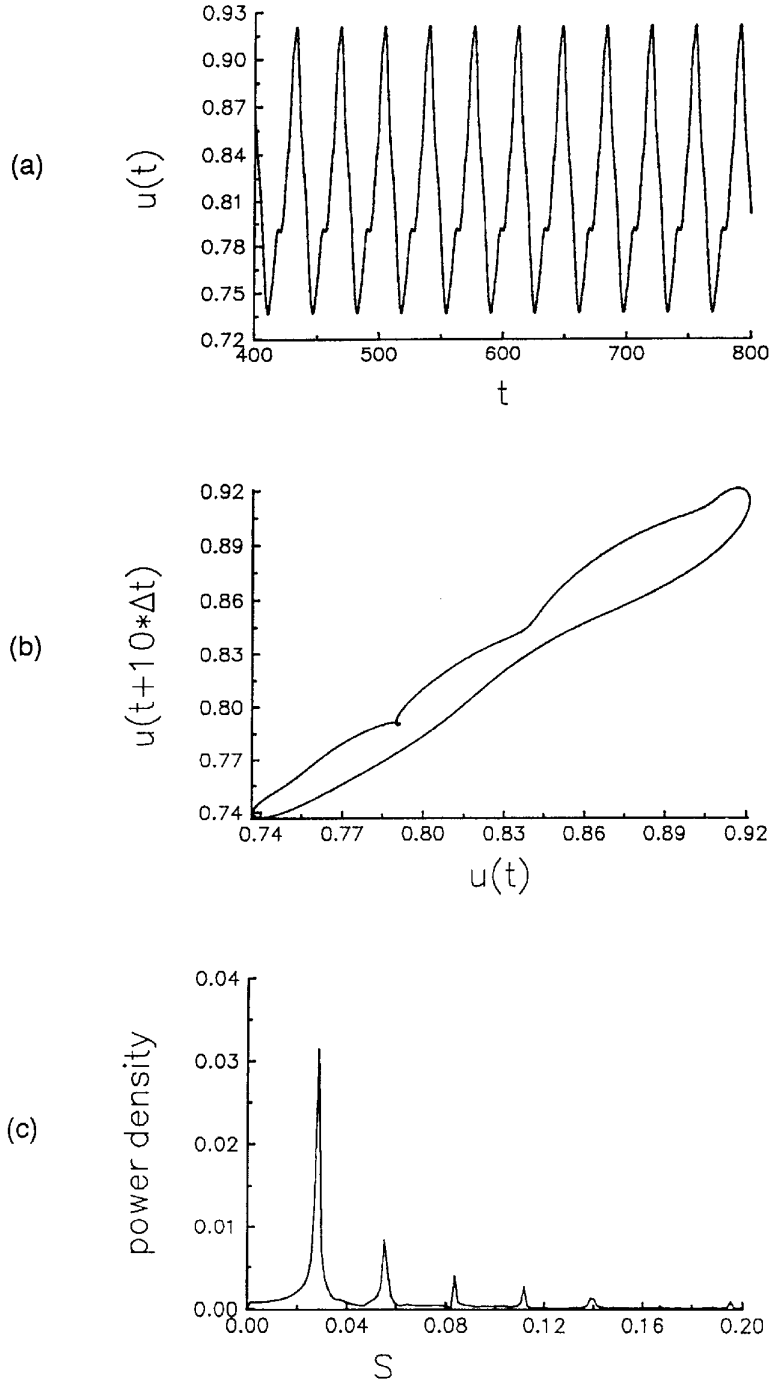

Figure 13. Velocity component $u(t)$ of radial jet for $Re = 220$: (a) time series; (b) time phase diagram; (c) Fourier analysis showing power density against Strouhal number S

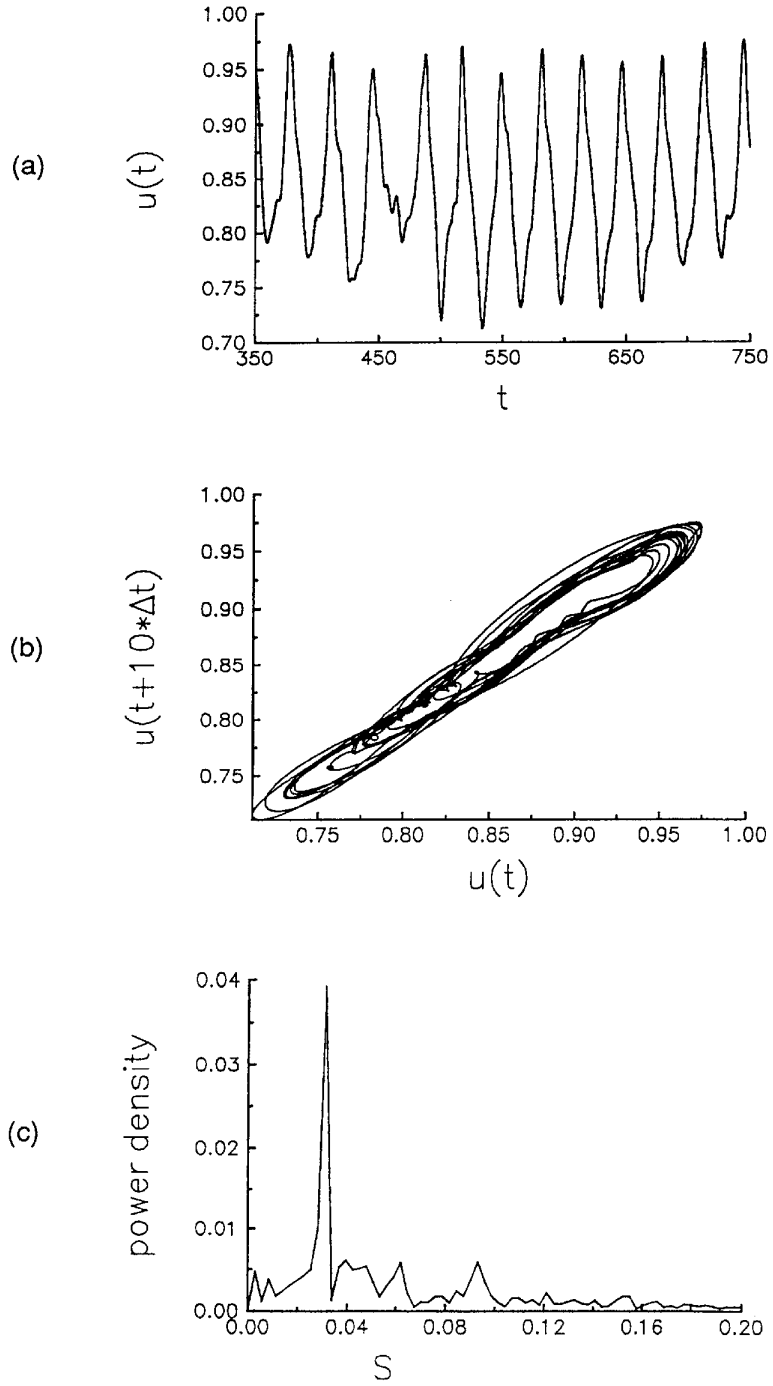

Figure 14. Velocity component $u(t)$ of radial jet for $Re = 230$: (a) time series; (b) time phase diagram; (c) Fourier analysis showing power density against Strouhal number S

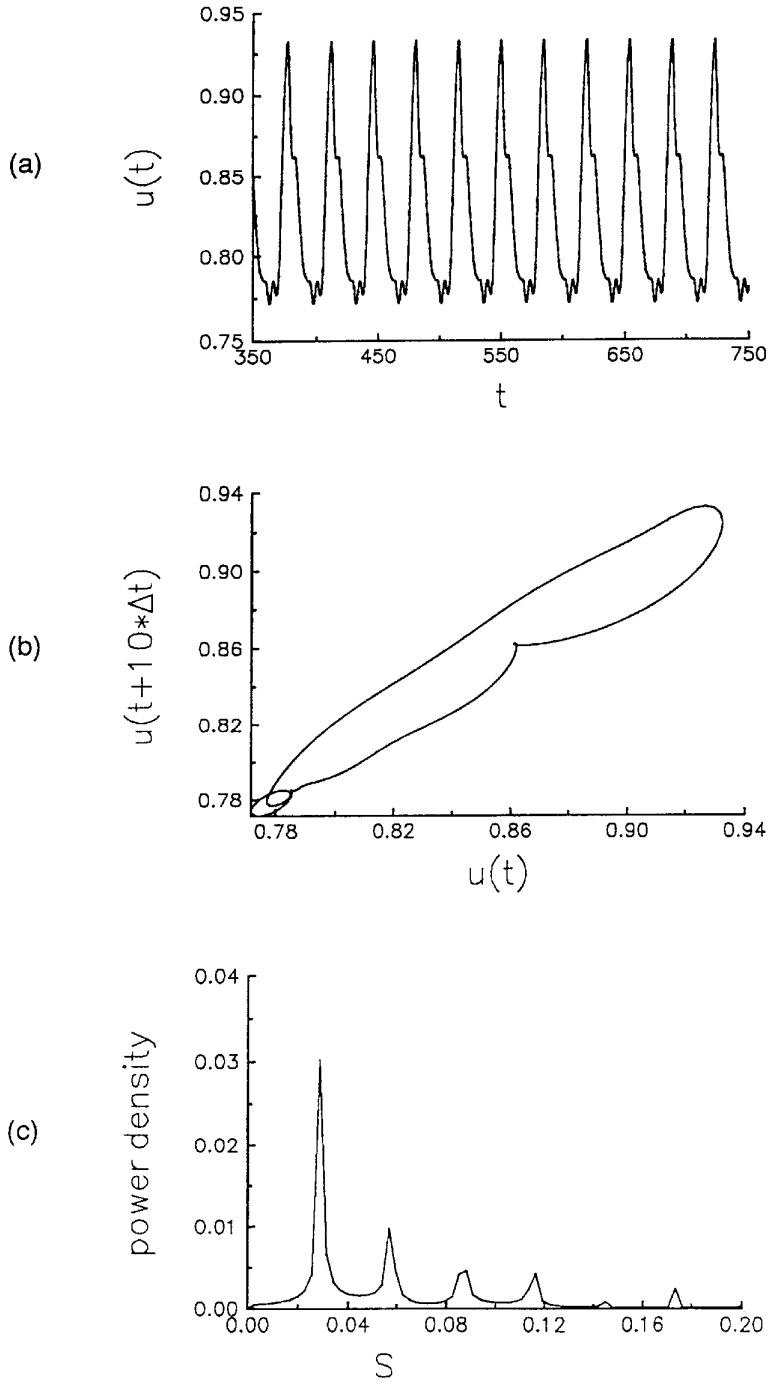

Figure 15. Velocity component $u(t)$ of radial jet for $Re = 240$: (a) time series; (b) time phase diagram; (c) Fourier analysis showing power density against Strouhal number S

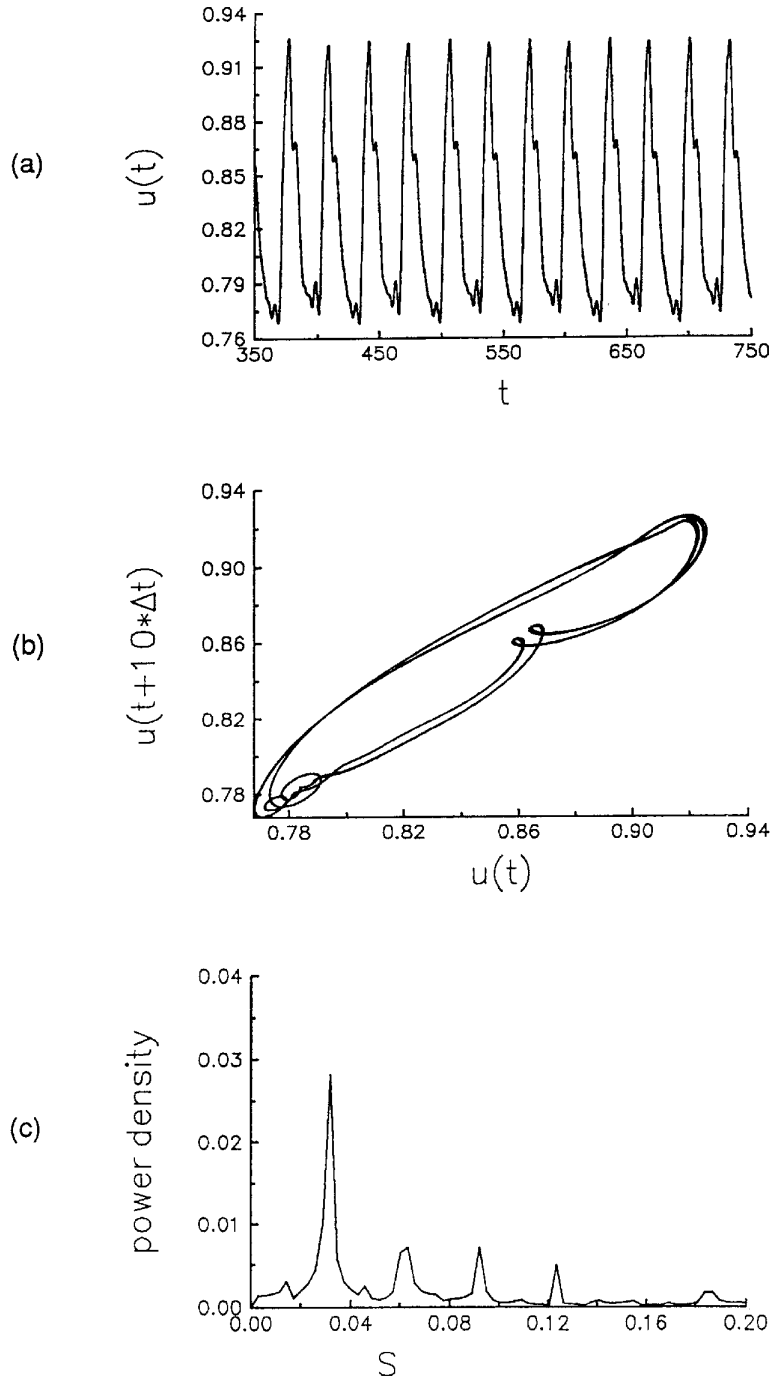

Figure 16. Velocity component $u(t)$ of radial jet for $Re = 245$: (a) time series; (b) time phase diagram; (c) Fourier analysis showing power density against Strouhal number S

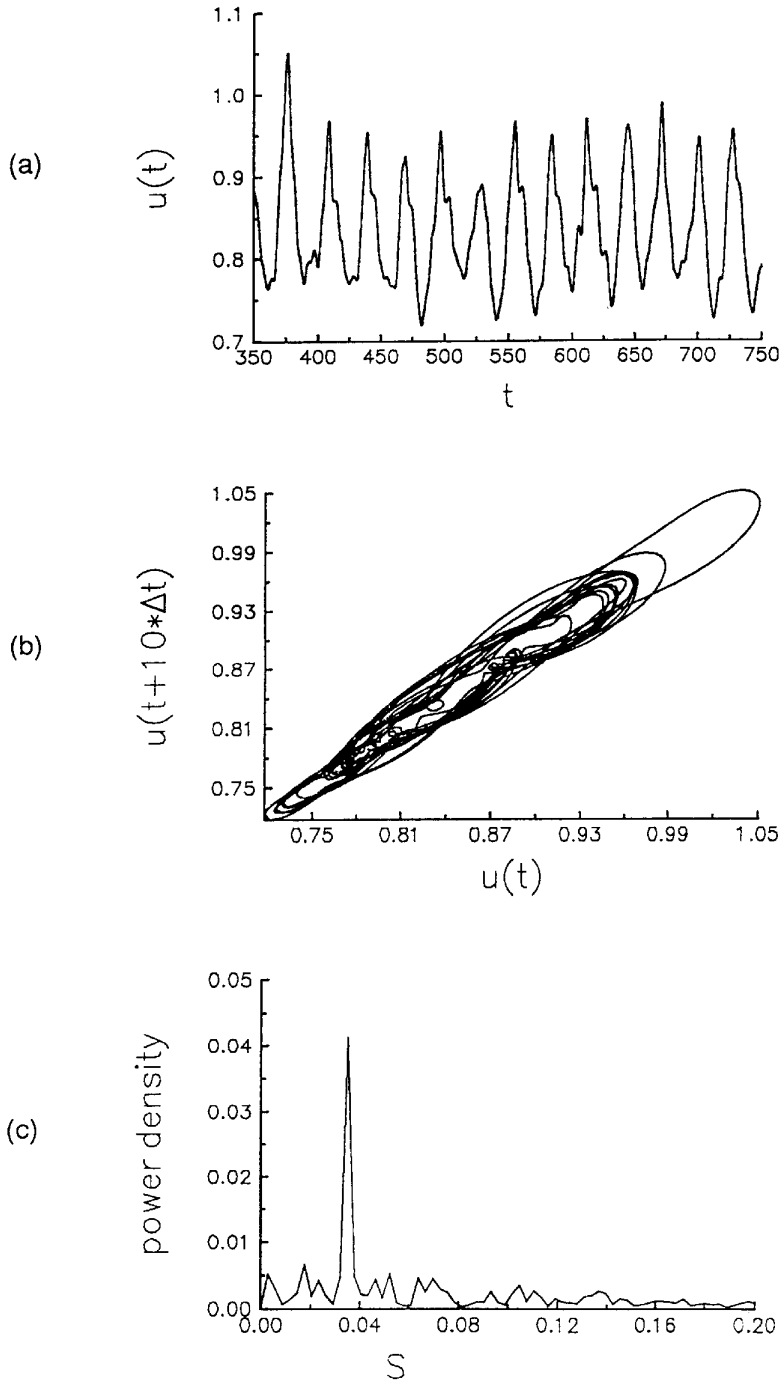

Figure 17. Velocity component $u(t)$ of radial jet for $Re = 250$: (a) time series; (b) time phase diagram; (c) Fourier analysis showing power density against Strouhal number S

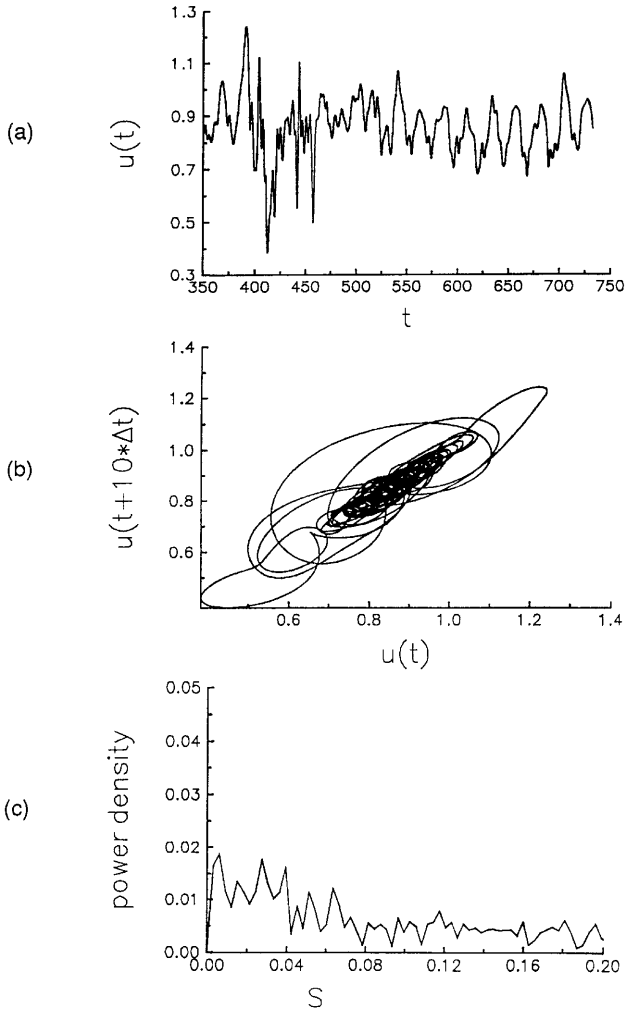

Figure 18. Velocity component $u(t)$ of radial jet for $Re = 275$: (a) time series; (b) time phase diagram; (c) Fourier analysis showing power density against Strouhal number S

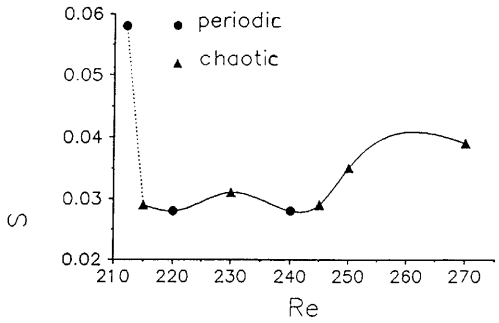

Figure 19. Dependence of dominant Strouhal number of radial jet on Reynolds number

REFERENCES

1. H. Schlichting, *Boundary-Layer Theory*, 7th edn, McGraw-Hill, New York, 1979.
2. H. Martin, 'Heat and mass transfer between impinging gas jets and solid surfaces', *Adv. Heat Transfer*, **13**, 1–60 (1977).
3. M. D. Deshpande and R. N. Vaishnar, 'Submerged laminar jet impingement on a plane', *J. Fluid Mech*., **114**, 213–236 (1982).
4. S. M. Hosseinalipour and A. S. Mujumdar, 'Comparative evalution of different turbulence models for confined impinging and opposing jet flows', *Numer. Heat Transfer A*, **28**, 647–666 (1995).
5. H. Laschefski, D. Braess, H. Haneke and N. K. Mitra, 'Numerical investigations of radial jet reattachment flows', *Int. j. numer. methods fluids*, **18**, 629–646 (1994).
6. M. Winkelsträter, H. Laschefski and N. K. Mitra, 'Transition to chaos in impinging three dimensional axial and radial jets', *Proc. 14th Int. Conf. on Numerical Methods in Fluid Dynamics*, Springer, Bangalore, 1994, pp. 368–371.
7. F. H. Pulliam and J. A. Vastano, 'Transition to chaos in an unforced 2D flow', *J. Comput. Phys*., **105**, 133–149 (1993).
8. C. R. Maliska and G. D. Raithby, 'A method for computing three dimensional flows using non-orthogonal boundary-fitted coordinates', *Int. j. numer. methods fluids*, **4**, 519–537 (1984).
9. J. P. van Doormal and G. D. Raithby, 'Enhancement of SIMPLE method for predicting incompressible fluid flows', *Numer. Heat Transfer*, **7**, 147–163 (1984).
10. H. Laschefski, T. Cziesla, G. Biswas and N. K. Mitra, 'Numerical investigation of heat transfer by rows of rectangular impinging jets', *Numer. Heat Transfer A*, **30**, 87–101 (1996).

